

Simulation of left ventricle fluid dynamics with mitral regurgitation from magnetic resonance images with fictitious elastic structure regularization

T. Lassila^{a *}, A.C.I. Malossi^b, M. Stevanella^c,
E. Votta^c, A. Redaelli^c and S. Deparis^a

Apr 20th, 2014

^a*Institute of Mathematics, EPFL, Lausanne, Switzerland;*

^b*IBM Research, Zürich, Switzerland;*

^c*Bioengineering Department, Politecnico di Milano, Milan, Italy*

Abstract

Computer modeling can provide quantitative insight into cardiac fluid dynamics phenomena that are not evident from standard imaging tools. We propose a new approach to modeling left ventricle fluid dynamics based on an image-driven model-based description of ventricular motion. In this approach, the end-diastolic geometry and time-dependent deformation of the left ventricle cavity are obtained from cardiac magnetic resonance images and a fictitious elastic structure is used to impose the contractile behavior of the left ventricle. This allows seamless treatment of the isovolumic phases. Besides the ventricular motion, the intracavitary fluid dynamics is controlled by the mitral valve. Three different mitral valve models are included in the simulation: an idealized diode (with or without regurgitation) and a lumped parameter model accounting for the opening dynamics of the valve and including regurgitation.

Keywords : fluid-structure interaction; left ventricular fluid dynamics; mitral regurgitation

1 Introduction

The high prevalence and rate of mortality of cardiac diseases have driven the development of methods to gain quantitative insight into cardiac function and, in particular, the function of the left ventricle (LV). Among the different aspects of LV biomechanics, intracavitary fluid dynamics plays a pivotal role and can provide a noninvasive indicator of different pathological conditions. In healthy LVs, the haemodynamics are characterized by: (i) *high intraventricular pressure gradients* during the early diastole (E-wave) that give rise to a 3-D vortex ring forming immediately downstream of the mitral valve (MV) leaflets and help generate a strong jet that extends all the way to the apex with minimal viscous dissipation; (ii) *sustained rotational flow* during late-diastolic atrial contraction (A-wave); and (iii) *rapid contraction* during systole that redirects the blood to the LV outflow tract and through the aortic valve. These features contribute to optimizing the LV pumping efficiency, as well as to the haemodynamics in the proximal aorta, and their alteration is usually associated with pathological conditions.

Computational fluid dynamics simulations can be useful for analyzing LV fluid dynamics to overcome the limitations of current imaging techniques. Due to the importance of the motion of the LV cavity and the MV leaflets, these fluid dynamics simulations should ideally be extended to fluid-structure interaction (FSI) simulations taking also into account the interplay between the biological tissue and moving blood. The setting of a fully realistic FSI model of the LV is particularly challenging, since it has to account for: i) the complex LV geometry; ii) the presence

of heart valves, whose modeling is non-trivial and is required to have realistic inflow and outflow boundary conditions; iii) the complex motion of the LV wall during the cardiac cycle. Such motion can be imposed either directly by means of kinematic boundary conditions on the boundary of the LV cavity, or through the explicit modeling of the LV myocardium, which requires the modeling of passive and active mechanical properties of myocardial tissue, of the laminar structure of the LV and its myocardial fiber architecture, and ultimately of the propagation of contraction. The latter approach is more demanding since it requires the identification of a large number of model parameters through complex experimental set-ups and procedures, as was done in [SCC⁺11] for patient-specific electromechanical models and in [WZC⁺10] for valve models.

Current medical imaging technology can yield the information required to reconstruct LV 3D geometry. For instance, cardiac magnetic resonance imaging (cMRI) can be performed with different acquisition sequences to quantify i) LV anatomy, time-dependent volume, and wall motion from cine images, ii) regional 2D wall motion and strains from tagged images, iii) local tissue necrosis/fibrosis from late gadolinium enhanced images, iv) myocardial fiber architecture from diffusion tensor cMRI, and v) blood velocity fields from phase contrast images. These data can be used to feed image-based, patient-specific FSI models, which can be used to study different aspects of LV biomechanics by means of morphologically realistic 3D models, as well as to test the suitability of different medical and surgical treatments on a patient-specific basis to support clinical planning. Still, only cine-cMRI and late gadolinium enhanced acquisitions are routinely performed in clinics, while the acquisition of the other sequences is usually limited to research activities due to their complex implementation and their excessive time for analysis.

With increased availability of image-based detailed information, many FSI studies have been performed in realistic LV geometries (see [COS05, DSR⁺09, LMX⁺08, NWY06, TYGdN10]), accounting also for LV wall electro-mechanics in some cases (see [NMK⁺11, WSKH04]). In such studies it is typically assumed that the effect of the MV leaflets is negligible and the MV is modelled by inflow boundary conditions that try to represent the time-varying shape and orientation of the MV orifice. In the literature, only recently have appeared fully three-dimensional fluid dynamics studies in patient-specific LV geometries incorporating the leaflet dynamics (see [MKKDL⁺13, MIS⁺11, VLS⁺13]), although a fully realistic model coupling unsteady haemodynamics effects with anisotropic material models for the leaflets with contact modelling and inclusion of the effects of chordae tendinae and the papillary muscles still seems out of reach. This aspect may appear of minor relevance, but is not: experimental evidence strongly suggests that motion of the MV leaflets and LV vorticity influence each other during diastole (see [CKS⁺13, KWP⁺95]), while computational studies indicate that the systolic configuration of the anterior MV leaflet plays a role in LV ejection efficiency [DCS⁺12].

In this work we present a novel approach to LV FSI modeling. Based on standard short-axis cine cMRI images an *in vivo* LV model-based geometry is reconstructed and regional LV wall 3D displacements are identified from the cMRI by an algorithm of [CVC⁺11]. Space- and time-dependent 3D-displacements are imposed to the LV endocardial surface through a thin fictitious elastic solid, so as to avoid difficulties related to exact volume conservation during the isovolumic phases. A MV model is introduced through three different approaches. In the first case the mitral valve is treated as an idealized diode that is either fully open or fully closed and provides no resistance to the flow. In the second case the ideal diode is modified to allow for regurgitation according to suitable and the valve resistance. In the third case a lumped parameter model accounts for the opening dynamics of the valve as proposed by [MDPS11] so that the resistance offered by the valve changes in time according to the pressure gradient across it. All three models also account for the up-and-down motion of the mitral annulus, but not for its resizing nor the effect of the immersed leaflets. A comparison between the fluid dynamics predictions is made in order to understand which implications the choice of the model has on the fluid dynamics predictions.

2 Methods

2.1 Image acquisition and motion reconstruction of the LV

The methodology was tested on imaging data from a 65-year-old female patient who had a hibernating myocardium in the LAD territory and volume overload due to mitral regurgitation; the septal side of the LV was severely akinetic. Using a 1.5 T whole-body Siemens Avantoa MRI scanner, equipped with a commercial cardiac coil, electrocardiogram-gated breath-hold cine images of the LV were acquired in multiple short axes using steady state free precession sequences (20 time frames/cardiac cycle, reconstruction matrix 256×256 pixels, in plane resolution 1.719×1.719 mm², slice thickness 8 mm, gap 1.6 mm). The valves and LV apex were not captured, due to the inherent limitations of the short-axis sequence. The imaging and reconstruction method are described in detail in [CVC⁺11], where a validation of the methodology was done by comparison to commercial software for CMR analysis, and is briefly summarized here. For every time frame and on each short-axis slice the LV endocardial contour was semi-automatically detected through the Chan-Vese approach and integrated with a priori knowledge of the statistical distribution of gray levels in medical images. Contours were regularized using a curvature-based motion algorithm designed to disallow curvatures above the mean Euclidean value. For each time frame, the smooth LV endocardial surface was obtained by biplanar cubic spline approximation of previously detected contours. The surface was discretized into approximately 2000 three-node triangular elements. In the end-diastolic frame, the endocardial surface was divided into six longitudinal sections and three circumferential sections, thus obtaining 18 sectors. For each sector, nine points forming a 3×3 mapped grid were identified and the corresponding local principal curvatures calculated as in [VS05]. Then, each point of each section was tracked throughout the subsequent time-points by means of a nearest neighbor search, based on the minimization of the frame-by-frame variations in spatial position and local curvature. The result of this procedure was the time-dependent position of 84 landmark points for the entire endocardial surface.

2.2 Patient-specific LV geometry for FSI simulations

A model-based approach for constructing a computational LV geometry was used. The LV intracavitary volume mesh was obtained by starting from an idealized tetrahedral mesh representing the general LV shape and then morphing it by nonrigid deformations to fit the short-axis landmark points in the end-diastolic configuration. To mimic the LV we used a truncated ellipsoid with short extruded sections extending from both valves, which were modelled as ellipsoidal surfaces. By an extrusion procedure a thin fictitious elastic structure around the endocardium was generated for the purposes of imposing the motion of the LV. The dimensions and alignment of the mitral valve long and short axis were fitted to those observed in the long-axis sequence. The mitral valve annulus was approximated by an ellipsoid with major axis 3.5 cm and minor axis 2.6 cm at peak systole, whereas the aortic valve was approximated by a circle of diameter 1.8 cm.

The idealized LV was aligned and resized to match the position of the landmarks at end-diastolic configuration of the anatomically correct LV reconstructed from MRI. First, we applied a rigid transformation to the idealized LV to align the vertices on the endocardium surface with the MRI-derived set of landmark points. Then, we defined a least-squares error functional measuring the discrepancy between the two sets of points and solved a least-square minimization problem to find the optimal scaling of the idealized LV in each of the three major axis directions. During this minimization process the volume of the LV was constrained to equal the MRI-based approximation and the total length of the LV was constrained to equal that observed in the long-axis sequence. The top-most short-axis slice was assumed to be located at a distance of 2 cm of length from the valvular plane.

After alignment and resizing, the ideal LV geometry was nonrigidly deformed to fit the landmark points. First, for each landmark point we identified the closest boundary mesh nodal point on the endocardium at end-diastole. Using this point-to-point identification an initial deformation was applied to the idealized LV using radial basis function interpolation that warped the ideal-

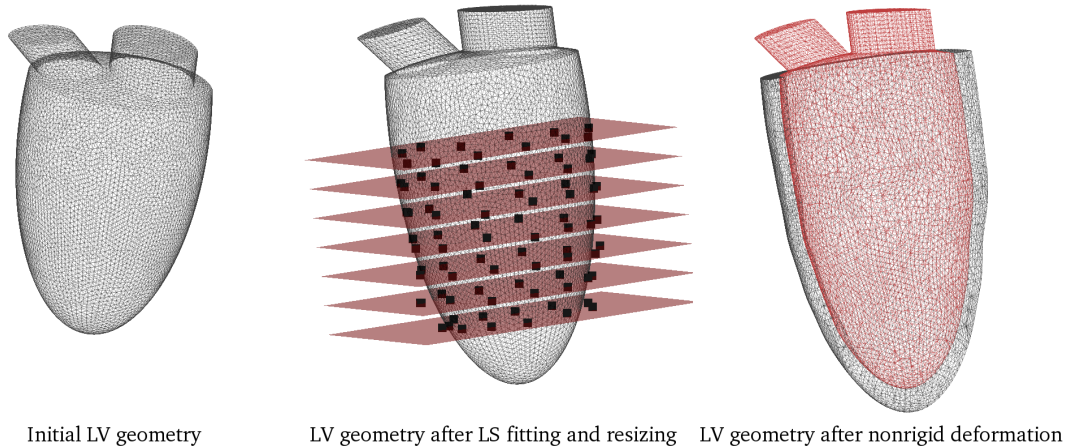


Figure 1: The idealized ellipsoidal LV geometry (left) is first aligned to the short-axis planes and landmarks. An affine transformation that minimizes the discrepancy between the landmarks and the endocardial surface is then sought by least-squares fitting (middle). In the final step a nonrigid radial basis function deformation is applied to both fluid and solid geometries to obtain the computational mesh (right).

ize LV endocardium to match the landmark points. This deformed configuration was then taken as the initial end-diastolic configuration. After the nonrigid deformation was applied to obtain the end-diastolic configuration that matched the position of the landmarks at the end-diastolic instant, the motion of the landmark points was extrapolated and used to drive the finite element simulation of the ventricular haemodynamics. The positions of the landmark points on the endocardium were chosen as interpolation centers, and the motion of the landmarks in space and time was extrapolated in the space-time domain by performing radial basis function interpolation in space and trigonometric interpolation in time. In order to regularize the motion, the five highest temporal modes were neglected so that the resulting LV volume reconstruction was monotone increasing during diastole. This resulted in a globally smooth and time-periodic extension field of the LV motion throughout one heartbeat. The procedure is illustrated in Fig. 1.

A separate long-axis sequence was used to register the mitral leaflets relative to the position of the aortic root. Two phases of the long-axis sequence were used for the mitral leaflet registration at diastolic (fully open) and systolic (closed but regurgitant) positions. This was performed manually by identifying 42–46 landmark points split between the two leaflets and least-squares fitting of two bivariate polynomial surfaces of total degree four for both leaflet surfaces. From this reconstruction the maximum opening area of the mitral valve was estimated at 7.22 cm^2 and the mitral regurgitant area was estimated at 0.07 cm^2 .

2.3 Finite element modelling of LV haemodynamics

Ventricular haemodynamics were modelled with a finite element FSI model. The fluid part of the FSI modeling problem consisted of the Navier-Stokes equations (NSE) for incompressible Newtonian fluids written in the arbitrary Lagrangian-Eulerian (ALE) formulation. The thin structure surrounding the LV was only used to impose the motion of the LV in such a way as to obtain smooth LV pressure fields both in space and time, and was thus modelled as a thin pseudo-incompressible linear elastic and isotropic material. In order to impose the reconstructed motion of the LV in the haemodynamics simulation, we used the extrapolated space-time motion field as a boundary condition on the external surface of the thin extruded structure surrounding the LV. The current study only focuses on LV haemodynamics and so no predictions of myocardial strains or stresses were needed, though these could have been obtained by replacing the thin linear isotropic structure with a physiologically motivated nonlinear orthotropic material of realistic

thickness. While there is extra computational cost related to the fluid-solid coupled problem, this formulation allowed both the recovery of a spatio-temporally smooth LV pressure field as well as the ability to seamlessly simulate both isovolumic phases, which are a known difficulty for the pure NSE-in-moving-domains -formulation (e.g. [CMN14] eliminate the isovolumic phases completely in an otherwise high-fidelity simulation of full-heart fluid dynamics).

The resulting FSI problem reads

$$\left\{ \begin{array}{l} \frac{\partial \mathbf{u}_F}{\partial t} \Big|_{\mathbf{x}^0} + \left(\left(\mathbf{u}_F - \frac{\partial \mathbf{d}_F}{\partial t} \Big|_{\mathbf{x}^0} \right) \cdot \nabla \right) \mathbf{u}_F - \frac{1}{\rho_F} \nabla \cdot \sigma_F = \mathbf{0} \quad \text{in } \Omega_F^t \times (0, T], \\ \nabla \cdot \mathbf{u}_F = 0 \quad \text{in } \Omega_F^t \times (0, T], \\ \rho_S \frac{\partial^2 \mathbf{d}_S}{\partial t^2} - \nabla \cdot \sigma_S = \mathbf{0} \quad \text{in } \Omega_S^0 \times (0, T], \\ -\Delta \mathbf{d}_F = \mathbf{0} \quad \text{in } \Omega_F^0 \times (0, T], \\ \mathbf{u}_F \circ \mathcal{M}^t - \frac{\partial \mathbf{d}_S}{\partial t} = \mathbf{0} \quad \text{on } \Gamma_I^0 \times (0, T], \\ \sigma_S \cdot \mathbf{n}_S - J_S \mathbf{G}_S^{-T} (\sigma_F \circ \mathcal{M}^t) \cdot \mathbf{n}_S = \mathbf{0} \quad \text{on } \Gamma_I^0 \times (0, T], \\ \mathbf{d}_F - \mathbf{d}_S = \mathbf{0} \quad \text{on } \Gamma_I^0 \times (0, T], \end{array} \right. \quad (1)$$

where $(0, T]$ is the time interval, \mathbf{u}_F the fluid velocity, ρ_F and ρ_S are the fluid and solid density, respectively, \mathbf{n}_S is the outgoing normal direction applied to the solid domain, $\mathbf{G}_S = \mathbf{I} + \nabla \mathbf{d}_S$ the solid deformation gradient (with \mathbf{I} the identity matrix), and $J_S = \det(\mathbf{G}_S)$. In addition, σ_F and σ_S are the Cauchy and the first Piola–Kirchhoff stress tensors. The motion of the interior vertices of the fluid mesh was obtained by harmonic extension from the FSI interface by solving an elliptic PDE.

2.4 Modelling of insufficient mitral valve dynamics

For the purposes of this study we performed the LV haemodynamics simulations with three different models for the mitral valve.

Model A: The classical model for cardiac valves is the ideal diode model, which offers no resistance to the blood flow and opens and closes instantaneously in response to the changing of the pressure gradient sign and flow direction:

$$Q_{mv} = \begin{cases} \frac{p_{pv} - p_{lv}}{R_{la}}, & \text{if } p_{pv} > p_{lv} \\ 0, & \text{if } p_{pv} \leq p_{lv} \end{cases}, \quad (2)$$

where p_{pv} and p_{lv} are the pulmonary and LV pressure respectively. In this model the mitral inflow rate Q_{mv} was imposed as a boundary condition on the FSI LV problem using Lagrange multipliers to enforce the defective boundary condition (see e.g. [FGNQ02]), which has the benefit that no explicit velocity profile needs to be imposed at the inflow. In order to stabilize the velocity at the mitral valve due to flow reversal effects, the tangential component of the velocity field at the inlet was further constrained to zero (see [MBH+11] and the discussion therein), leading to the inflow boundary condition:

$$\int_{\Gamma_{in}} \mathbf{u}_F \cdot \mathbf{n} \, d\Gamma = 0, \quad (\mathbf{I} - \mathbf{n}\mathbf{n}^T) \mathbf{u} = \mathbf{0} \quad \text{on } \Gamma_{in}. \quad (3)$$

Model B: Is an extension of Model A that incorporates regurgitation and inertial effects of the valve on the fluid dynamics. In this model the flow rate is given by the Bernoulli's equation for flow through an orifice:

$$p_{pv} - p_{lv} = R_{la} Q_{mv} + B Q_{mv} |Q_{mv}| + L \frac{dQ_{mv}}{dt} \quad (4)$$

where $B = \rho/(2A_{\text{eff}}^2)$ is the Bernoulli resistance of the valve and $L = \rho \ell_{\text{eff}}/A_{\text{eff}}$ the blood inertance. The coefficients L and B are determined by the effective orifice area A_{eff} that switches between open and closed valve configurations similarly to the ideal diode case:

$$A_{\text{eff}} = \begin{cases} A_{\text{max}}, & \text{if } p_{\text{pv}} > p_{\text{lv}} \\ A_{\text{min}}, & \text{if } p_{\text{pv}} \leq p_{\text{lv}} \end{cases}. \quad (5)$$

For $A_{\text{min}} > 0$ the model allows regurgitation to take place. The maximum and minimum orifice area were calibrated from the long-axis segmentation of the valve geometry and were estimated as $A_{\text{max}} = 7.22 \text{ cm}^2$ and $A_{\text{min}} = 0.07 \text{ cm}^2$ respectively, for the case studied. A numerically stable time discretization was obtained for (4) by using the semi-implicit scheme

$$Q_{\text{mv}}^{n,k} = \frac{Q_{\text{mv}}^{n-1} + \frac{\Delta t}{L} (p_{\text{la}}^{n,k-1} - p_{\text{lv}}^{n,k-1})}{1 + \Delta t B/L |Q_{\text{mv}}^{n-1}|}. \quad (6)$$

In this model the pressure p_{lv} was imposed as a normal stress boundary condition on the FSI LV problem along with the aforementioned tangential velocity stabilization condition:

$$(\sigma_{\text{F}} + p_{\text{lv}}\mathbf{I})\mathbf{n} = \mathbf{0} \text{ on } \Gamma_{\text{in}}, \quad (\mathbf{I} - \mathbf{nn}^T)\mathbf{u} = \mathbf{0} \text{ on } \Gamma_{\text{in}}. \quad (7)$$

Model C: To model more precisely the valve opening dynamics we used a lumped parameter model proposed by [MDPS11], which prescribes simple and smooth opening and closing dynamics for A_{eff} without explicitly modeling the valve leaflets. In this model the flow rate through the mitral valve is again given by Bernoulli's equation (4) for flow through an orifice, which in turn depends on an internal variable $\zeta \in [0, 1]$ according to

$$A_{\text{eff}}(t) = [A_{\text{max}} - A_{\text{min}}]\zeta(t) + A_{\text{min}}, \quad (8)$$

where the internal variable evolves according to the rate equation

$$\frac{d\zeta}{dt} = \begin{cases} (1 - \zeta)K_{vo}(p_{\text{la}} - p_{\text{lv}}), & \text{if } p_{\text{la}} \geq p_{\text{lv}} \\ \zeta K_{vc}(p_{\text{la}} - p_{\text{lv}}), & \text{if } p_{\text{la}} \leq p_{\text{lv}} \end{cases}. \quad (9)$$

This model captures the valve opening dynamics and represents mitral insufficiency, but does not model the effect of the leaflets on the local flow pattern. The boundary conditions applied on the FSI LV problem were identical to (7).

2.5 Ventricular pre- and afterload

A scenario of chronic mitral regurgitation with a constant pulmonary pressure of $p_{\text{pv}} = 10 \text{ mmHg}$ was chosen for the preload. For the ventricular afterload we used a standard three-element windkessel model with the parameters given by [SWW99] to determine the aortic flow rate Q_{ao} and aortic pressure p_{ao} as:

$$\frac{dQ_{\text{ao}}}{dt} = \frac{1}{R_{\text{ao}}R_{\text{pe}}C_{\text{ao}}} \left[R_{\text{pe}}C_{\text{ao}} \frac{d}{dt}(p_{\text{ao}} - p_{\text{ve}}) + (p_{\text{ao}} - p_{\text{ve}}) - (R_{\text{pe}} + R_{\text{ao}})Q_{\text{ao}} \right], \quad (10)$$

where R_{ao} is the aortic resistance, R_{pe} is the peripheral resistance, and C_{ao} is the aortic compliance. The venous pressure p_{ve} was fixed at 5 mmHg. All of values of the model parameters used are listed in Table 1. Model A was used for the aortic valve in all three cases. It is also possible to model the aortic valve similarly to the mitral one, though this was not deemed necessary in the presence of a healthy aortic valve. For the coupling algorithm between the 3D LV model with the windkessel model for the ventricular afterload, we refer to [MBDQ11, MBD12, MBC+13].

3 Results

The LV FSI simulation was initialized at rest with zero velocity and pressure and driven for a few heartbeats at 75 bpm until pressure conditions stabilized into periodicity. The pulmonary pressure was ramped to 10 mmHg in the course of the first 100 ms of the simulation to provide an impulse-free initialization, then kept constant for the rest of the run. No further initializations or regularizations needed to be performed. A fixed time step of 1 ms was used for the solution of the FSI problem with second-order backward differentiation formula in time. The finite element problem was discretized using 124 942 tetrahedral elements in the fluid domain and piecewise linear basis functions for both velocity and pressure approximation. Well-posedness of the problem was guaranteed by convective and pressure stabilization performed with the interior penalty method by [BFH06]. The peak Reynolds number inside the LV during the diastolic phase was around 2 000, indicating transitional but not fully turbulent flow, and therefore no turbulence modelling was performed.

The velocity field and the diastolic jet for each of the three different valve models A, B and C is presented in Fig. 2 for three different time instances: early diastole, late diastole and early systole. In all three cases the diastolic jet is strongly driven towards the lateral wall and generates a large vortex near the aortic root that expands to fill the entire LV during the late diastolic A-wave. These features are independent of the inflow boundary condition applied (flow rate in Model A and pressure in Models B and C) and the opening dynamics of the MV. All three models exhibited vortical flow at the mitral inlet during early systole, but the numerical simulation remained stable and convergent throughout, indicating a successful stabilization of the inlet boundary condition during flow reversal.

The mitral valve opening ratio, LV pressure and LV volume in time for the three different valve Models A, B and C are presented in Fig. 3. Model A stands apart from the other two due to the absence of mitral regurgitation, leading to larger systolic pressure and delayed opening of the MV by about 10 ms. The MV inflow is strongly bimodal and the A-wave is considerably stronger than the E-wave, which is consistent with clinical findings of chronic or compensated mitral regurgitation when the left atrium has to compensate for the diminished filling of the LV. Again, very little quantitative difference between Models B and C can be observed in terms of pressure and flow rate. This can be explained by the fact that the inflow/outflow volumetric flow rates are largely constrained by the imposed motion of fictitious elastic structure that follows from the 4-D reconstruction.

Table 2 shows the regurgitant volume and its fraction of the total systolic outflow, the ejection fraction and the viscous dissipation. The predicted regurgitant volume is 9% higher in Model C, mainly due to the slower closure of the mitral valve. Peak viscous dissipation during systole was slightly higher in Model A without regurgitation, but almost identical across all three models during diastole. The prediction of viscous dissipation depends mainly on whether or not regurgitation is considered or not.

4 Discussion

In this work we presented a computational method starting from a standard short-axis MRI sequence and proceeding to a 4-D reconstruction of LV motion combined with FSI simulations using a fictitious elastic structure for regularization. A model-based approach was used to generate the LV computational geometry. The use of short-axis images permitted a streamlined workflow from images to simulations with minimal user intervention. The motion of the basal cutplane was added in order to obtain sufficient ejection fraction and to recover the downward motion of the LV that was missing from the short-axis images. The mitral annulus diameter orifice area were calibrated according to manual long-axis segmentation of the LV.

Compared to standard Navier-Stokes-in-moving-domain formulations, the FSI formulation treats seamlessly the isovolumic phases without need for explicit volume preservation constraints on the imposed LV motion. Thus the entire cardiac cycle was simulated in one continuous run

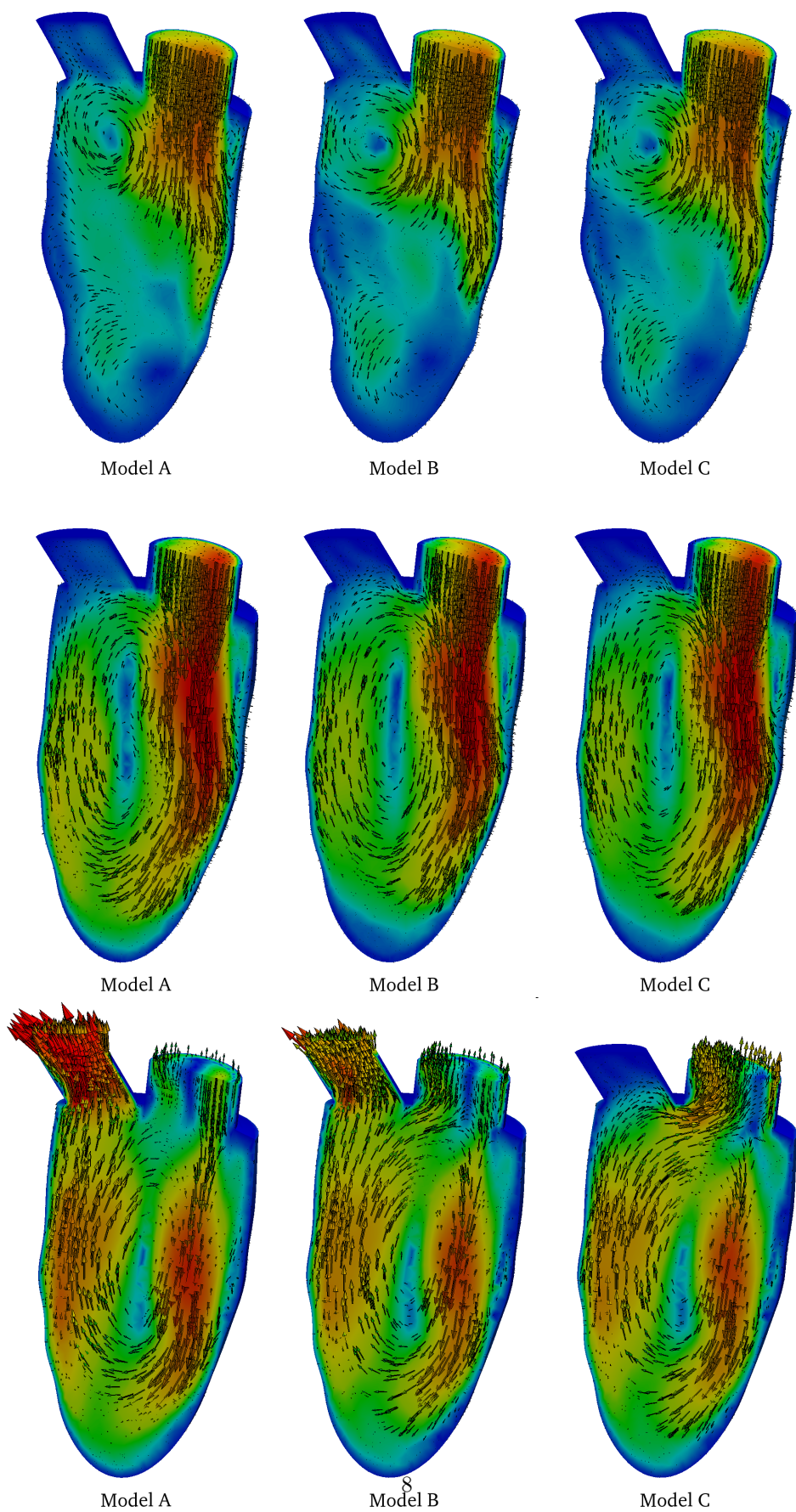


Figure 2: Comparison of vortex jets for the Models A, B and C. Top row: early diastolic velocity ($t = 550$ ms). Middle row: late diastolic velocity ($t = 750$ ms). Bottom row: early systolic velocity ($t = 800$ ms). Color bar ranges between 0 – 40 cm/s.

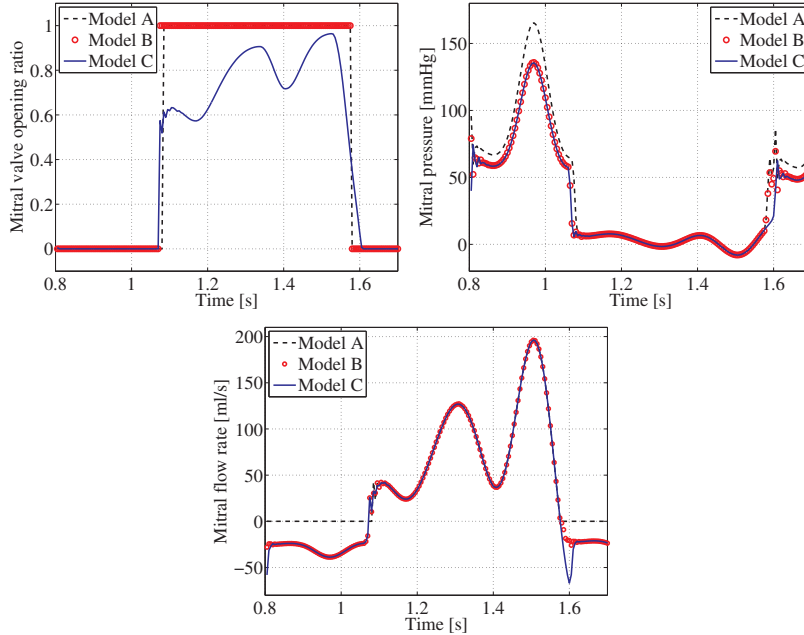


Figure 3: Comparison of mitral valve characteristics for the valve Models A, B and C. The absence of mitral regurgitation in Model A leads to an increase of 19% in the prediction of systolic pressure peak pressure. The difference between the simple regurgitant valve (Model B) and the dynamic regurgitant valve (Model C) is negligible in terms of pressure and flow rate.

without needing to change boundary conditions or enforcing isovolumic constraints when switching from systole to diastole and vice versa.

Comparison of the three different simplified MV models produced qualitatively similar diastolic flow patterns. A nonsymmetric fluid jet created a two-phase vorticity pattern where a small vortex was generated near the posterior mitral leaflet in the E-wave and during the A-wave a large vortex developed to fill the entire LV cavity. Addition of the lumped parameter valve dynamics by themselves had little effect on the observed LV flow, provided the mitral regurgitation was properly accounted for, and neither had the change in the LV FSI boundary condition from average flow rate condition to pressure condition. The fact that consistent results were obtained across all the valve models used indicates that LV vortical flow patterns may be simulated to some extent with just knowledge of the LV wall motion.

Limitations of the current simulation study include the lack of explicit leaflet modelling and their effect on the inflow jet, lack of variability of the orifice shape and size, and the missing information about the orientation of the left atrium with respect to the MV, which influences the diastolic jet orientation and consequently the vorticity pattern (as shown by [SM13]). While the approximate configuration of the mitral valve geometry can be obtained from the MRI in the fully open and fully closed position, extending this information to the intermediate configurations and simulating the effect of the leaflet motion to the flow in a proper way requires further work. Furthermore, solving the problem in the FSI formulation introduces certain additional complexities in the preconditioning and solution algorithms that may not always be available in commercial software.

Acknowledgements

Clinical patient data for this study was provided by the team of Prof. O. Parodi at Ospedale Niguarda, Milan, Italy. S. Deparis, T. Lassila, A. Redaelli, M. Stevanella, and E. Votta acknowl-

edge the support of the European Community 7th Framework Programme, Project FP7-224635 VPH2 (‘Virtual Pathological Heart of the Virtual Physiological Human’). A. C. I. Malossi and S. Deparis acknowledge the European Research Council Advanced Grant ‘Mathcard, Mathematical Modeling and Simulation of the Cardiovascular System’, Project ERC-2008-AdG 227058, as well as the Swiss Platform for High-Performance and High-Productivity Computing (HP2C). All of the numerical results presented in this paper have been computed using the LGPL LifeV library (www.lifev.org). All authors disclose no conflicts of interest.

References

- [BFH06] E. Burman, M. A. Fernández, and P. Hansbo. Continuous interior penalty finite element method for Oseen’s equations. *SIAM J. Numer. Anal.*, 44(3):1248–1274, 2006.
- [CKS⁺13] J. J. Charonko, R. Kumar, K. Stewart, W. C. Little, and P. P. Vlachos. Vortices formed on the mitral valve tips aid normal left ventricular filling. *Ann. Biomed. Eng.*, pages 1–13, 2013.
- [CMN14] C. Chnafa, S. Mendez, and F. Nicoud. Image-based large-eddy simulation in a realistic left heart. *Comput. Fluids*, 2014. DOI: 10.1016/j.compfluid.2014.01.030.
- [COS05] Y. Cheng, H. Oertel, and T. Schenkel. Fluid-structure coupled CFD simulation of the left ventricular flow during filling phase. *Ann. Biomed. Eng.*, 33(5):567–576, 2005.
- [CVC⁺11] C. A. Conti, E. Votta, C. Corsi, D. De Marchi, G. Tarroni, M. Stevanella, M. Lombardi, O. Parodi, E. G. Caiani, and A. Redaelli. Left ventricular modelling: a quantitative functional assessment tool based on cardiac magnetic resonance imaging. *J. R. Soc. Interface*, 1(3):384–395, 2011.
- [DCS⁺12] A. Dimasi, E. Cattarinuzzi, M. Stevanella, C. A. Conti, E. Votta, F. Maffessanti, N. B. Ingels Jr, and A. Redaelli. Influence of mitral valve anterior leaflet in vivo shape on left ventricular ejection. *Cardiovasc. Engr. Tech.*, 3(4):388–401, 2012.
- [DSR⁺09] T. Doenst, K. Spiegel, M. Reik, M. Markl, J. Hennig, S. Nitzsche, F. Beyersdorf, and H. Oertel. Fluid-dynamic modeling of the human left ventricle: methodology and application to surgical ventricular reconstruction. *Ann. Thorac. Surg.*, 87(4):1187–1195, 2009.
- [FGNQ02] L. Formaggia, J.-F. Gerbeau, F. Nobile, and A. Quarteroni. Numerical treatment of defective boundary conditions for the Navier–Stokes equations. *SIAM J. Numer. Anal.*, 40(1):376–401, 2002.
- [KWP⁺95] W.Y. Kim, P.G. Walker, E.M. Pedersen, J.K. Poulsen, S. Oyre, K. Houliand, and A.P. Yoganathan. Left ventricular blood flow patterns in normal subjects: A quantitative analysis by three-dimensional magnetic resonance velocity mapping. *J. Am. Coll. Cardiol.*, 26:224–238, 1995.
- [LMX⁺08] Q. Long, R. Merrifield, X. Y. Xu, P. Kilner, D. N. Firmin, and G. Z. Yang. Subject-specific computational simulation of left ventricular flow based on magnetic resonance imaging. *P. I. Mech. Eng. H*, 222(4):475, 2008.
- [MBC⁺13] A. C. I. Malossi, P. J. Blanco, P. Crosetto, S. Deparis, and A. Quarteroni. Implicit coupling of one-dimensional and three-dimensional blood flow models with compliant vessels. *SIAM J. Multiscale Model. Simul.*, 11(2):474–506, 2013.
- [MBD12] A. C. I. Malossi, P. J. Blanco, and S. Deparis. A two-level time step technique for the partitioned solution of one-dimensional arterial networks. *Comp. Meth. Appl. Mech. Engrg.*, 237–240:212–226, 2012.
- [MBDQ11] A. C. I. Malossi, P. J. Blanco, S. Deparis, and A. Quarteroni. Algorithms for the partitioned solution of weakly coupled fluid models for cardiovascular flows. *Int. J. Num. Meth. Biomed. Engrg.*, 27(12):2035–2057, 2011.
- [MBH⁺11] M.E. Moghadam, Y. Bazilevs, T.-Y. Hsia, I.E. Vignon-Clementel, and A.L. Marsden. A comparison of outlet boundary treatments for prevention of backflow divergence with relevance to blood flow simulations. *Comput. Mech.*, 48:277–291, 2011.
- [MDPS11] J. P. Mynard, M. R. Davidson, D. J. Penny, and J. J. Smolich. A simple, versatile valve model for use in lumped parameter and one-dimensional cardiovascular models. *Int. J. Num. Meth. Biomed. Engrg.*, 28(6–7):626–641, 2011.

- [MIS⁺11] V. Mihalef, R. I. Ionasec, P. Sharma, B. Georgescu, I. Voigt, M. Suehling, and D. Comaniciu. Patient-specific modelling of whole heart anatomy, dynamics and haemodynamics from four-dimensional cardiac CT images. *J. R. Soc. Interface*, 1(3):286–296, 2011.
- [MKKDL⁺13] J. O. Mangual, E. Kraigher-Krainer, A. De Luca, L. Toncelli, A. Shah, S. Solomon, G. Galanti, F. Domenichini, and G. Pedrizzetti. Comparative numerical study on left ventricular fluid dynamics after dilated cardiomyopathy. *J. Biomech.*, pages 1611–1617, 2013.
- [NMK⁺11] D. Nordsletten, M. McCormick, P. J. Kilner, P. Hunter, D. Kay, and N. P. Smith. Fluid–solid coupling for the investigation of diastolic and systolic human left ventricular function. *Int. J. Numer. Methods Biomed. Engr.*, 27(7):1017–1039, 2011.
- [NWX06] M. Nakamura, S. Wada, and T. Yamaguchi. Influence of the opening mode of the mitral valve orifice on intraventricular hemodynamics. *Ann. Biomed. Eng.*, 34(6):927–935, 2006.
- [SCC⁺11] M. Sermesant, R. Chabiniok, P. Chinchapatnam, T. Mansi, F. Billet, P. Moireau, J. M. Peyrat, K. Wong, J. Relan, K. Rhode, et al. Patient-specific electromechanical models of the heart for the prediction of pacing acute effects in CRT: A preliminary clinical validation. *Medical Image Anal.*, 16(1):201–215, 2011.
- [SM13] J.H. Seo and R. Mittal. Effect of diastolic flow patterns on the function of the left ventricle. *Phys. Fluids*, 25(11):110801, 2013.
- [SWW99] N. Stergiopoulos, B. Westerhof, and N. Westerhof. Total arterial inertance as the fourth element of the windkessel model. *Am. J. Physiol.*, 276(1):H81–H88, 1999.
- [TYGdN10] D. Tang, C. Yang, T. Geva, and P. J. del Nido. Image-based patient-specific ventricle models with fluid-structure interaction for cardiac function assessment and surgical design optimization. *Progr. Pediatr. Cardiol.*, 30(1–2):51–62, 2010.
- [VLS⁺13] E. Votta, T.B. Le, M. Stevanella, L. Fusini, E.G. Caiani, A. Redaelli, and F. Sotiropoulos. Toward patient-specific simulations of cardiac valves: State-of-the-art and future directions. *J. Biomech.*, 46(2):217–228, 2013.
- [VS05] M. Vieira and K. Shimada. Surface mesh segmentation and smooth surface extraction through region growing. *Comput. Aided Geom. D.*, 22(8):771–792, 2005.
- [WSKH04] H. Watanabe, S. Sugiura, H. Kafuku, and T. Hisada. Multiphysics simulation of left ventricular filling dynamics using fluid-structure interaction finite element method. *Biophys. J.*, 87(3):2074–2085, 2004.
- [WZC⁺10] J. F. Wenk, Z. Zhang, G. Cheng, D. Malhotra, G. Acevedo-Bolton, M. Burger, T. Suzuki, D. A. Saloner, A. W. Wallace, J. M. Guccione, and M. B. Ratcliffe. First finite element model of the left ventricle with mitral valve: insights into ischemic mitral regurgitation. *Ann. Thorac. Surg.*, 89(5):1546–1553, 2010.

Table 1: Main parameters of the global problem

ρ_F	Blood density	1.060 g cm ⁻³
μ_F	Blood dynamic viscosity	0.035 g cm ⁻¹ s ⁻¹
R_{la}	Left atrium resistance	0.09 mmHg s cm ⁻³
R_{ao}	Aortic resistance	0.03 mmHg s cm ⁻³
R_{pe}	Peripheral resistance	0.7 mmHg s cm ⁻³
C_{ao}	Aortic compliance	2 cm ³ mmHg ⁻¹
ℓ	Effective length	1 cm
K_{vo}	Rate coefficient, opening	0.04
K_{vc}	Rate coefficient, closure	0.03
p_{ve}	Venous pressure	5 mmHg
p_{pv}	Pulmonary pressure	10 mmHg
ρ_S	Solid density	1.2 g cm ⁻³
E_S	Solid Young’s modulus	0.7 MPa
ν_S	Solid Poisson’s ratio	0.48

Table 2: Global indicators of mitral regurgitation as predicted by the different models

Model	Regurgitant volume [ml]	Regurgitant fraction [%]	Ejection fraction [%]	Peak viscous dissipation [mW]
A	0.00	0.0%	28.9%	5.46 (s) / 0.666 (d)
B	8.02	19.7%	29.0%	4.21 (s) / 0.657 (d)
C	8.73	21.5%	28.9%	4.21 (s) / 0.659 (d)